PHOSPHONIC ACID MODIFICATION TO MOLYBDENUM ATOM CATALYST FOR CO_2 HYDROGENATION ON MAGNESIUM HYDRIDE SURFACE

Gumawa Windu Manggada[1,2] and Shixue Zhou[2]

[1]Department of Chemical Engineering, Politeknik Negeri Malang, Soekarno-Hatta Street No. 9, Malang 65141, Indonesia

[2]College of Chemical and Biological Engineering, Shandong University of Science and Technology, 579 Qianwangang Road, Qingdao 266590, China

gumawawindu@gmail.com; [zhoushixue66@163.com]

ABSTRACT

Catalytic hydrogenation is one of the most effective ways to convert CO_2 to high value-added chemicals, and it is challenging to improve the catalytic activity and product selectivity based on the understanding of catalysis mechanism of the process. In this work, organic phosphonic acid was innovatively employed to tune single atom catalyst for CO_2 hydrogenation to methanol, and the effect of fluoromethylphosphonic acid (FMPA) on the electronic structure of molybdenum and the reaction energy barriers of CO_2 hydrogenation on MgH_2 surface were investigated by density functional theory (DFT) calculations. The results showed that the reaction energy barriers at the key steps were significantly decreased by the introduction of FMPA, which stabilized the reaction intermediates from CO_2 hydrogenation by reducing the electron density of molybdenum adsorption site with its oxygen atoms. The reverse water gas shift (RWGS) pathway was superior to formate pathway for CO_2 hydrogenation on $FMPA/Mo-MgH_2(001)$ surface with energy barrier only 1.22 eV at the rate-determining step, and CH_3OH was the overwhelming product rather than $HCOOH$, H_2CO, CO or CH_4 considering the reaction barriers and adsorption energies. The combination of organic phosphonic acid with single atom catalyst can generate the rational design of new catalytic system, which is helpful to control the reaction pathway and product selectivity.

Keywords: carbon dioxide conversion, catalytic hydrogenation, magnesium hydride, organic phosphonic acid, single atom catalyst.

1. INTRODUCTION

Carbon dioxide can be used for the synthesis of synthesized into high value-added chemicals as a promising route to reduce greenhouse gas emissions and expand syngas resources [1-3]. Among the various approaches, thermo-catalytic hydrogenation technology is received significant attention [4-6]. Although many studies on CO_2 hydrogenation have been conducted, controlling product selectivity is still challenging.

The yield and selectivity of a product from CO_2 hydrogenation are determined by the reaction pathway. There are two possible reaction pathways, the formate pathway and the reverse water gas shift (RWGS) pathway, for CO_2 hydrogenation in terms of the first

---

hydrogenation step of CO_2 to form $HCOO^*$ or $COOH^*$ [7, 8]. In the formate pathway, the reaction begins with a H atom approaching the C atom of CO_2 molecule through the formation of formate ($HCOO^*$), followed by intermediate products formic acid (HCOOH) and formaldehyde (H_2CO) then final product methanol (CH_3OH) or methane (CH_4) [9-12]. The RWGS begins with a H atom approaching the O atom of CO_2 and involves the production of carbon monoxide (CO), and then goes on further hydrogenation [13-15].

Magnesium hydride is a prospected candidate for hydrogen storage, and it can be employed for hydrogenation, due to its abundant resources, low cost, and adjustable hydrogen releasing temperature [2, 16-19]. In this work, MgH_2 was used as hydrogen source for hydrogenation by directly providing active H atom from crystal lattice, instead of high-pressure hydrogen gas. On the other hand, efficient catalysts are necessary to reduce the activation energy of the stable C=O bonds in CO_2 [12, 20]. Single-atom catalyst (SAC) has attracted much research interest due to its high activity and efficiency [21-23]. In addition, phosphonic acid was reported for the catalysis of methanol conversion [24] and olefin production [25].

This work innovatively aimed to investigate the application of molybdenum single atom catalyst modified with organic phosphonic acid for CO_2 hydrogenation on MgH_2 surface using density functional theory (DFT) calculations. The adsorption of the reaction intermediates and the energy barrier of each elementary step involved in the CO_2 hydrogenation were calculated so that the minimum energy pathway (MEP) was determined. The clarification of the underlying function mechanism in the catalytic activity and product selectivity of CO_2 hydrogenation helps the rational design of an efficient catalytic system.

2. COMPUTATIONAL METHOD

The DFT calculations were performed using program package $DMol^3$ of software Materials Studio (Accelrys Software Inc.). The Perdew-Burke-Ernzerhof (PBE) functional of the generalized gradient approximation (GGA) was employed for the nonlocal exchange and correlation functional, and the electron wave function was based on double numerical plus polarization (DNP) to expand the valence electron function into numerical orbital for calculation accuracy [26]. DFT Semi-core pseudopotential was employed for the core treatment of electrons which represent core electrons by a single effective potential. The computational parameters were tolerance 1×10^{-6} Ha/atom for self-consistent field (SCF) and thermal smearing 0.01 Ha for quick convergence of orbital occupation, and energy tolerance 1.0×10^{-5} Ha/atom, maximum force gradient 0.002 Ha/Å, and maximum atomic displacement 0.005 Å for structure optimization.

The MgH_2(001) surface was constructed by a periodic three atomic layers of (3×3) unit cell slab with totally 27 Mg and 54 H atoms and separated by a vacuum gap of 20 Å to avoid periodic boundary interactions in all cases (Figure 1a), in which it was verified that the relativity of properties and reaction energy barriers calculated from three atomic layers was consistent with seven atomic layers. The bottom two atom layers were fixed to represent the optimized bulk positions, while others were allowed to relax together with an adsorbate. Brillouin-zone integrations were performed on a grid of 8×8×12 Monkhorst-Pack

k-mesh for unit cell optimization, and 2×2×1 for supercells. An Mo atom catalyst was loaded on the MgH$_2$(001) surface by replacing a Mg atom on the first layer, and fluoromethylphosphonic acid (FMPA) was introduced on the surface to complete the construction of substrate as shown in Figure 1b.
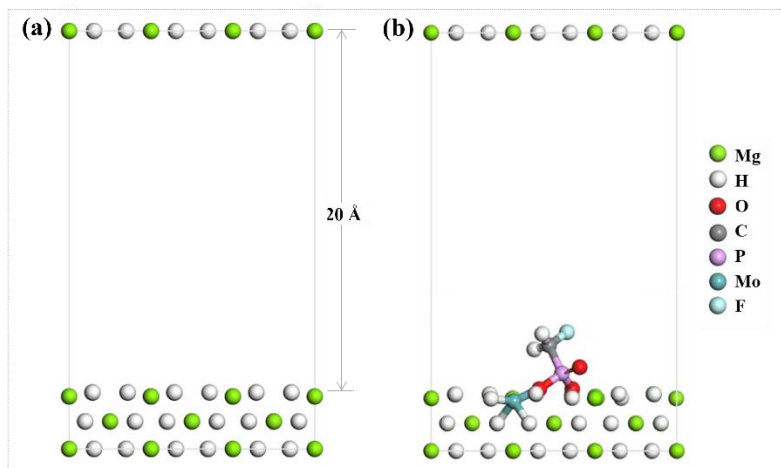
Figure 1. Structural models of (a) MgH$_2$(001) supercell and (b) substrate with Mo and FMPA.

The adsorption energy (E_{ads}) was calculated as follows:

$$E_{ads} = E_{adsorbate+substrate} - (E_{adsorbate} + E_{substrate}) \tag{1}$$

where $E_{adsorbate+substrate}$, $E_{adsorbate}$, and $E_{substrate}$, are the total energy of the substrate covered with adsorbate, adsorbate, and bare substrate, respectively [11, 27, 28].

The complete LST/QST (linear synchronous transit and quadratic synchronous transit) method was applied to identify the transition state configurations and to calculate relevant energy barriers of elementary steps involved in CO$_2$ hydrogenation reaction. The energy barrier (E_b) and the reaction energy (ΔE) were defined as below:

$$E_b = E_{TS} - E_{IS} \tag{2}$$
$$\Delta E = E_{FS} - E_{IS} \tag{3}$$

where E_{TS}, E_{IS}, and E_{FS} are the total energy of the transition state (TS), initial state (IS), and final state (FS), respectively [11].

3. RESULTS AND DISCUSSION

3.1 Effect of molybdenum atom and phosphonic acid on CO$_2$ adsorption and primary hydrogenation reactions

The stable adsorption configurations of CO$_2$ molecule on clean MgH$_2$(001) surface and the surfaces with Mo atom and FMPA were shown in Figure 2. On clean MgH$_2$(001) surface, CO$_2$ molecule was far away from the surface. In contrast, on Mo-MgH$_2$(001) and FMPA/Mo-MgH$_2$(001) surfaces, CO$_2$ molecule combined with Mo atom to form C-Mo and O-Mo bonds. The adsorption energies of CO$_2$, intermediates COOH[*], CO, and HCO[*] on different surfaces were listed in Table 1. High adsorption energies on Mo-MgH$_2$(001) and FMPA/Mo-MgH$_2$(001) surfaces were considered capable of weakening chemical bonds of the adsorbates so that the reaction energy barriers became lower.

MgH₂(001)   **Mo-MgH₂(001)**   **FMPA/Mo-MgH₂(001)**
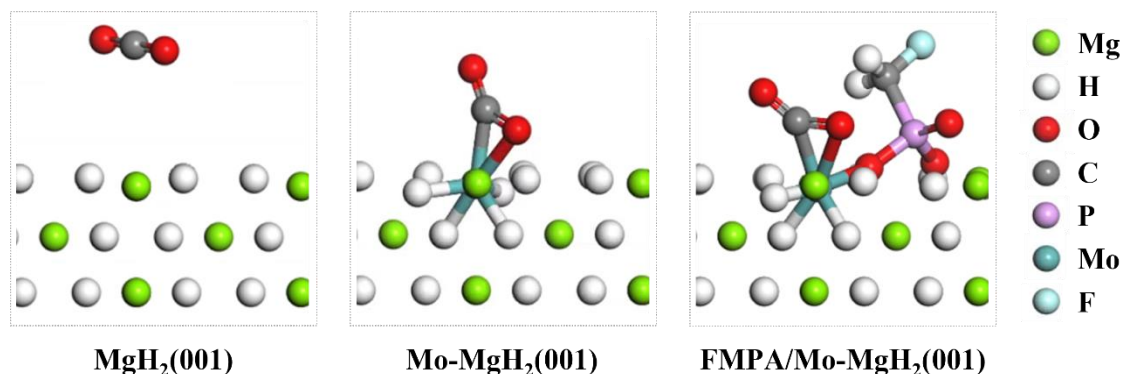
Figure 2. Optimized structures of CO_2 adsorption on MgH₂(001), Mo-MgH₂(001) and FMPA/Mo-MgH₂(001) surfaces

Table 1. Adsorption energies of key adsorbates in CO_2 hydrogenation on MgH₂(001), Mo-MgH₂(001) and FMPA/Mo-MgH₂(001) surfaces.

Adsorbate	E_{ads} on surface (eV)		
	MgH₂(001)	Mo-MgH₂(001)	FMPA/Mo-MgH₂(001)
CO_2	-0.09	-3.22	-2.38
COOH*	-1.13	-3.58	-4.56
CO	-0.57	-3.14	-3.22
HCO*	-0.98	-5.48	-5.30

The energy barriers of key hydrogenation reaction steps on different surfaces were listed in

Table 2. Some elementary steps were hindered by high energy barriers, such as COOH* formation and dissociation on MgH₂(001) surface and HCO* formation on Mo-MgH₂(001) surface, and the introduction of phosphonic acid reduced the reaction energy barriers.

Table 2. Energy barriers of elementary steps for CO_2 hydrogenation on MgH₂(001), Mo-MgH₂(001) and FMPA/Mo-MgH₂(001) surfaces.

Adsorbate	E_b on surface (eV)		
	MgH₂(001)	Mo-MgH₂(001)	FMPA/Mo-MgH₂(001)
CO_2+H* → COOH*	1.44	1.05	0.98
COOH* → CO+OH*	1.62	0.73	0.66
CO+H* → HCO*	1.04	1.92	1.22

The catalysis of Mo and phosphonic acid was clarified by the deformation charge density distribution and Mulliken atomic charge and the partial density of states (PDOS) analysis of intermediate COOH* on FMPA/Mo-MgH₂(001) surface compared with clean MgH₂(001) surface (Figure 3). On FMPA/Mo-MgH₂(001) surface, Mo atom provided electron density to the antibonding orbital of intermediate COOH* and accepted electron density from the bonding orbital of COOH* simultaneously as shown in Figure 3 (c).

Strong hybridization was found between C atom of intermediate COOH[*] (C 2s, 2p) and Mo 4d orbital at -2.55 eV on the left of Fermi level and 1.12 eV on the right of Fermi level. It is indicated as the bonding-antibonding pair and referred to the strong chemisorption, as shown in Figure 3 (d), which is in line with the theoretical study in reference [29]. Whereas, the interaction between COOH* and clean MgH_2(001) surface was weak, as shown in Figure 3 (a) and (b).
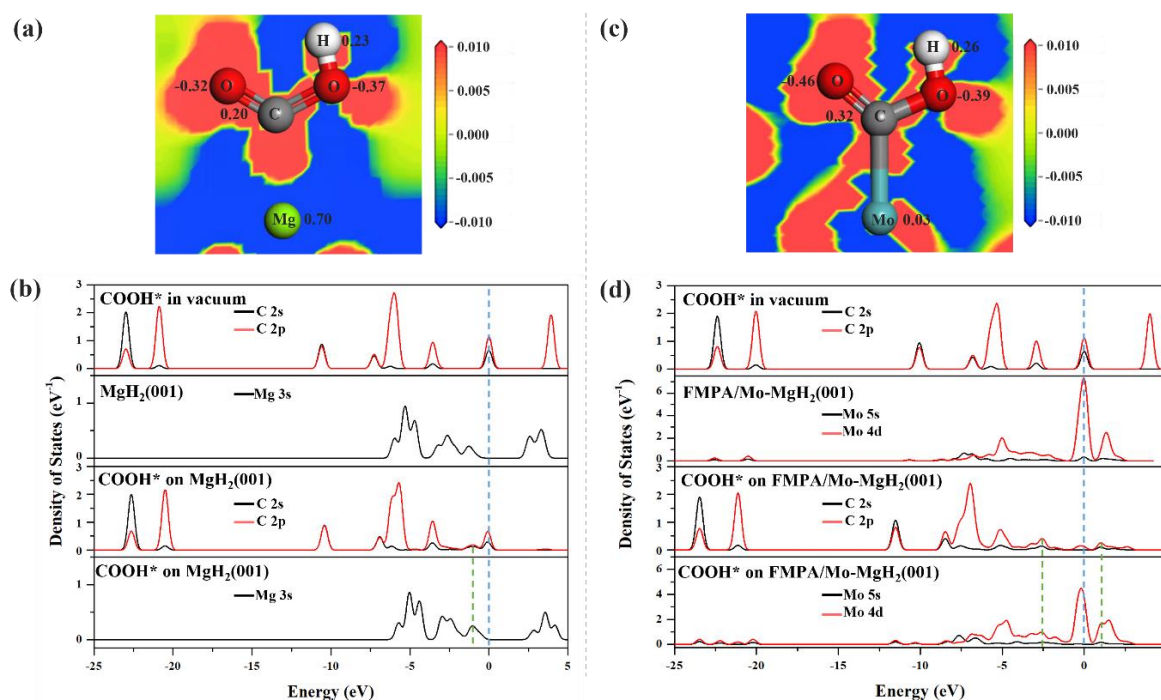
Figure 3. Deformation charge density and Mulliken atomic charge distribution (a and c) and PDOS profile (b and d) of COOH* on clean MgH_2(001) surface and FMPA/Mo-MgH_2(001) surface.

3.2 Reaction Pathway on FMPA/Mo-MgH_2(001) surface

Two possible reaction pathways, including RWGS and formate pathway for CO_2 hydrogenation, have been considered in this work to further understand the catalytic performance of FMPA/Mo-MgH_2(001) system and identify the rate-determining step (RDS), in which the pathway had a lower energy barrier of RDS. The overall reaction network is illustrated in Figure 4.

319
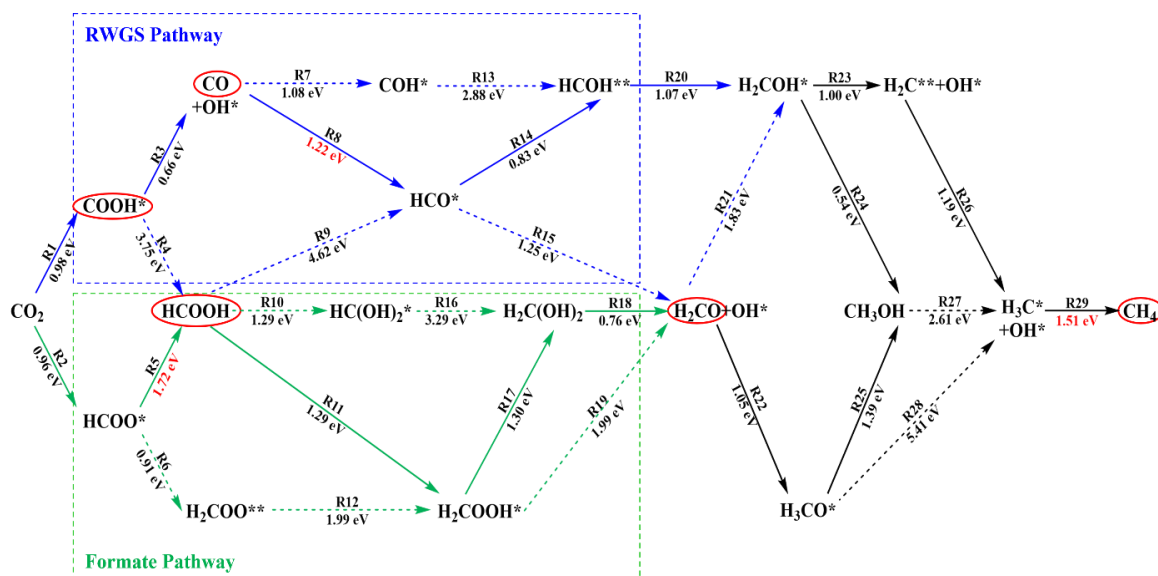
Figure 4. Reaction network and energy barriers for CO_2 hydrogenation on FMPA/Mo-MgH$_2$(001) surface. The asterisk (*) denotes uncoupled electron.

3.2.1 RWGS pathway on FMPA/Mo-MgH$_2$(001) surface

At the beginning of RWGS pathway (Figure 4), a H atom bound to the C atom of CO_2 to form COOH* with an energy barrier of 0.98 eV and exothermic energy of -1.94 eV. There were two possible routes for COOH* further reaction. It could be hydrogenated to the C atom to form HCOOH (R4) and further hydrogenated following the formate pathway. Unfortunately, the reaction was hindered by high energy barrier of 3.75 eV. So, the other route in which the dissociation of COOH* into CO with energy barrier only 0.66 eV was preferred. The hydrogenation of CO intermediate to form CH_3OH could be approached in four different ways. First, the hydrogenation of CO was initiated by the formation of O-H bond to form COH*, then COH* was hydrogenated to form HCOH**, H_2COH*, and CH_3OH (R7-R13-R20-R24). Second, a H atom was attracted by C atom to form HCO*, then followed the same route as in the first way to CH_3OH (R8-R13-R20-R24). Two other ways were both hydrogenation from CO to produce HCO* then intermediate H_2CO; one of which was followed by the formation of an H-O bond to form H_2COH* and then CH_3OH (R8-R15-R21-R24), and another was followed by H-C bond formation to form H_3CO* and CH_3OH (R8-R15-R22-R25). The energy barriers of rate-determining step in the four different ways were 2.88, 1.22, 1.83, and 1.39 eV, respectively. Thus, the second route through HCO* and HCOH** was the most favorable for the formation of CH_3OH.

Based on the reaction network, methane was the full hydrogenation product of CO_2 through the hydrogenation of intermediate H_3C* with energy barrier of 1.51 eV (R29). For the formation of H_3C*, three possible routes were considered. The first route was obtained from the dissociation of H_2COH* to H_2C** and OH* and followed by H_2C** hydrogenation to H_3C* (R23-R26), which was hampered by energy barrier of 1.19 eV at the rate-determining step. The second route was generated by the C-OH bond breakup of CH_3OH with an energy barrier of 2.61 eV (R27). The third possible route was hindered by

the high barrier of 5.41 eV from H_3CO^* hydrogenation and dissociation to produce H_3C^* and OH^*.

Comparing with CH_4 production, methanol was more readily produced from the hydrogenation of CO_2 on FMPA/Mo-MgH$_2$(001) surface via RWGS pathway according to the RDS analysis. The minimum energy path of RWGS pathway from CO_2 to CH_3OH on FMPA/Mo-MgH$_2$(001) surface was shown in Figure 5. The rate-determining step was the HCO^* formation, which is consistent with the calculation result in reference [30], whereas the energy barrier was much lower, 1.22 eV here versus 1.50 eV on Pd/TiO$_2$.
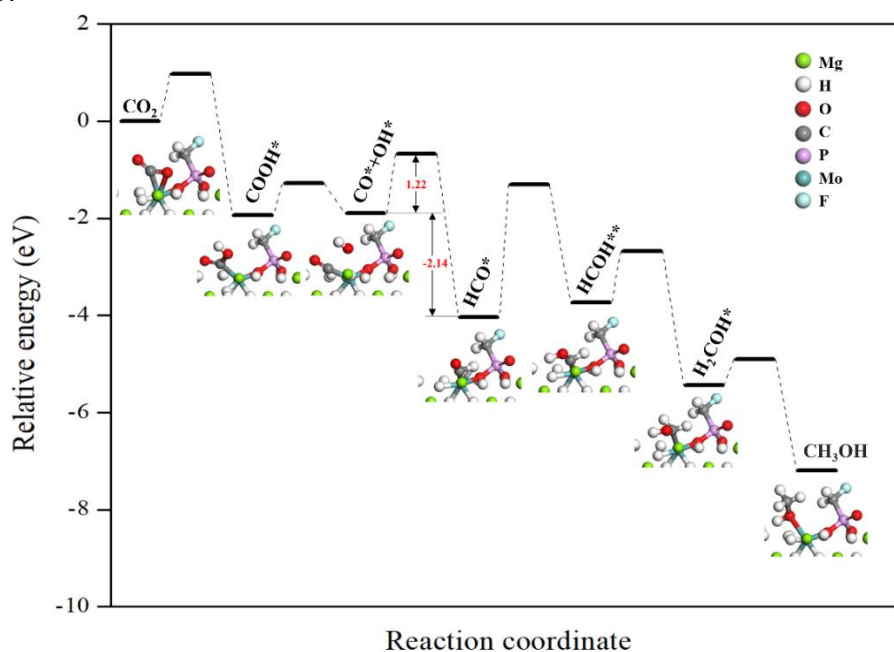
Figure 5. Minimum energy path of RWGS pathway for CO_2 hydrogenation on FMPA/Mo-MgH$_2$(001) surface.

3.2.2 Formate pathway on FMPA/Mo-MgH$_2$(001) surface

Formate pathway was characterized by the formation of intermediate formate ($HCOO^*$). On FMPA/Mo-MgH$_2$(001) surface, $HCOO^*$ was produced by the hydrogenation of CO_2 when a H attacked the C atom of CO_2 to form a C-H bond (R2) with an energy barrier of 0.79 eV and exothermic energy of -2.80 eV. The possible routes for $HCOO^*$ further hydrogenation had 1.72 eV energy barrier at rate-determining step. Therefore, in comparison with RWGS pathway on FMPA/Mo-MgH$_2$(001) surface, formate pathway was not favorable to the production of CH_3OH, which is consistent with the calculation result on Rh-doped Cu(111) surface in reference [31].

3.3 Rate-determining steps of CO_2 hydrogenation for different C_1 products on FMPA/Mo-MgH$_2$(001) surface

The adsorption energies, rate-determining steps, energy barriers, and reaction energies of C_1 products from CO_2 hydrogenation on FMPA/Mo-MgH$_2$(001) surface were summarized in

Table 3. Through RWGS pathway, the energy barrier of RDS for CO_2 to CO was only 0.98 eV, but the releasing of CO was hindered by high adsorption energy of CO. The further hydrogenation of CO was easy to produce methanol with energy barrier of 1.22

eV. For methane formation, the energy that was needed to overcome the barrier was more than 1.83 eV. On the other hand, the energy barrier of RDS via formate pathway to form formic acid, formaldehyde, and methanol was 1.72, 1.30, and 1.39 eV, respectively. Therefore, methanol was preferred as the main C_1 product of CO_2 hydrogenation on $FMPA/Mo-MgH_2(001)$ surface.

Table 3. Adsorption energies, rate-determining steps, and activation energies of C_1 products from CO_2 hydrogenation on $FMPA/Mo-MgH_2(001)$ surface.

Product	E_{ads} (eV)	Reaction	Rate-determining step	E_b (eV)	ΔE (eV)
CO	-3.22	$CO_2 \rightarrow CO$	$CO_2+H^* \rightarrow COOH^*$	0.98	-1.93
HCOOH	-0.97	$CO_2 \rightarrow HCOOH$	$HCOO^*+H^* \rightarrow HCOOH$	1.72	-0.75
H_2CO	-3.77	$CO \rightarrow H_2CO$	$HCO^*+H^* \rightarrow H_2CO$	1.24	-1.93
		$HCOOH \rightarrow H_2CO$	$H_2COOH^*+H^* \rightarrow H_2C(OH)_2$	1.30	-1.39
CH_3OH	-1.38	$CO \rightarrow CH_3OH$	$CO+H^* \rightarrow HCO^*$	1.22	-2.14
		$H_2CO \rightarrow CH_3OH$	$H_3CO^*+H^* \rightarrow CH_3OH$	1.39	-1.19
CH$_4$	-0.38	$CO \rightarrow CH_4$	$H_3C^*+H^* \rightarrow CH_4$	1.51	-1.76
		$CH_3OH \rightarrow CH_4$	$CH_3OH \rightarrow H_3C^* + OH^*$	2.61	-0.01
		$H_2CO \rightarrow CH_4$	$H_2CO+H^* \rightarrow H_2COH^*$	1.83	-1.13

4. CONCLUSION AND SUGGESTIONS

The introduction of organic phosphonic acid to molybdenum single atom catalyst on MgH_2 surface for CO_2 hydrogenation effectively lowered the reaction energy barriers. Organic phosphonic acid decreased the electron density at molybdenum atom adsorption site and enhanced the stability of reaction intermediates and transition states in CO_2 hydrogenation, and therefore it decreased the reaction energy barriers. On $FMPA/Mo-MgH_2(001)$ surface, the RWGS pathway was superior to formate pathway with high selectivity of methanol as the C_1 product for CO_2 hydrogenation.

This study will inspire the design of new catalytic system in single atom catalyst by tuning the electron structure with organic phosphonic acid to decrease the reaction energy barrier and improve product selectivity. However, both the selection of a transition metal atom and the functional group of organic phosphonic acid should be optimized for a specific reaction product.

ACKNOWLEDGEMENTS

REFERENCES

[1] Y. Zheng, W. Zhang, Y. Li, J. Chen, B. Yu, J. Wang, L. Zhang, J. Zhang, Energy related CO_2 conversion and utilization: Advanced materials/nanomaterials, reaction mechanisms and technologies, *Nano Energy*, 40, 512-539, 2017.

[2]   H. Chen, P. Liu, J. Liu, X. Feng, S. Zhou, Mechanochemical in-situ incorporation of Ni on MgO/MgH_2 surface for the selective O-/C-terminal catalytic hydrogenation of CO_2 to CH_4, *Journal of Catalysis*, 394, 397-405, 2020.

[3]   T.R. Anderson, E. Hawkins, P.D. Jones, CO_2, the greenhouse effect and global warming: from the pioneering work of Arrhenius and Callendar to today's Earth System Models, *Endeavour*, 40, 178-187, 2016.

[4]   M. Aresta, A. Dibenedetto, A. Angelini, Catalysis for the valorization of exhaust carbon: from CO_2 to chemicals, materials, and fuels. Technological use of CO_2, *Chemical Reviews*, 114, 1709-1742, 2014.

[5]   Q. Pan, J. Peng, S. Wang, S. Wang, In situ FTIR spectroscopic study of the CO_2 methanation mechanism on $Ni/Ce_{0.5}Zr_{0.5}O_2$, *Catalysis Science & Technology*, 4, 502-509, 2014.

[6]   P.A.U. Aldana, F. Ocampo, K. Kobl, B. Louis, F. Thibault-Starzyk, M. Daturi, P. Bazin, S. Thomas, A.C. Roger, Catalytic CO_2 valorization into CH_4 on Ni-based ceria-zirconia. Reaction mechanism by operando IR spectroscopy, *Catalysis Today*, 215, 201-207, 2013.

[7]   Y. Yang, J. Evans, J.A. Rodriguez, M.G. White, P. Liu, Fundamental studies of methanol synthesis from CO_2 hydrogenation on Cu(111), Cu clusters, and Cu/ZnO(0001), *Physical Chemistry Chemical Physics*, 12, 9909-9917, 2010.

[8]   S. Kattel, P. Ramírez, J. Chen, J. Rodriguez, P. Liu, Active sites for CO_2 hydrogenation to methanol on Cu/ZnO catalysts, *Science*, 355, 1296-1299, 2017.

[9]   J. Ye, C. Liu, D. Mei, Q. Ge, Active oxygen vacancy site for methanol synthesis from CO_2 Hydrogenation on In_2O_3(110): A DFT Study, *ACS Catalysis*, 3, 1296-1306, 2013.

[10]   Y.-F. Zhao, R. Rousseau, J. Li, D. Mei, Theoretical study of syngas hydrogenation to methanol on the polar Zn-terminated ZnO(0001) surface, *The Journal of Physical Chemistry C*, 116, 15952-15961, 2012.

[11]   L. Liu, X. Su, H. Zhang, N. Gao, F. Xue, Y. Ma, Z. Jiang, T. Fang, Zirconia-modified copper catalyst for CO_2 conversion to methanol from DFT study, *Applied Surface Science*, 528, 146900, 2020.

[12]   Z. Ou, C. Qin, J. Niu, L. Zhang, J. Ran, A comprehensive DFT study of CO_2 catalytic conversion by H_2 over Pt-doped Ni catalysts, *International Journal of Hydrogen Energy*, 44, 819-834, 2019.

[13]   A.G. Kharaji, A. Shariati, M.A. Takassi, A novel γ-alumina supported Fe-Mo bimetallic catalyst for reverse water gas shift reaction, *Chinese Journal of Chemical Engineering*, 21, 1007-1014, 2013.

[14]   L. Wang, S. Zhang, Y. Liu, Reverse water gas shift reaction over Co-precipitated Ni-CeO_2 catalysts, *Journal of Rare Earths*, 26, 66-70, 2008.

[15]   W. Wang, Y. Zhang, Z. Wang, J.-M. Yan, Q. Ge, C.-J. Liu, Reverse water gas shift over In_2O_3-CeO_2 catalysts, *Catalysis Today*, 259, 402-408, 2016.

[16]   S. Zhou, Q. Zhang, H. Chen, X. Zang, X. Zhou, R. Wang, X. Jiang, B. Yang, R. Jiang, Crystalline structure, energy calculation, and dehydriding thermodynamics of magnesium hydride from reactive milling, *International Journal of Hydrogen Energy*, 40, 11484-11490, 2015.

[17]   H. Chen, N. Ma, J. Li, Y. Wang, C. She, Y. Zhang, X. Li, J. Liu, X. Feng, S. Zhou, Effect of atomic iron on hydriding reaction of magnesium: Atomic-substitution and atomic-adsorption cases from a density functional theory study, *Applied Surface Science*, 504, 144489, 2020.

[18]   H. Chen, Z. Han, X. Feng, P. Liu, J. Liu, G. Liu, W. Yuan, T. Ren, S. Zhou, Solid-phase hydrogen in a magnesium-carbon composite for efficient hydrogenation of carbon disulfide, *Journal of Materials Chemistry A*, 6, 3055-3062, 2018.

[19]   P. Selvam, B. Viswanathan, C.S. Swamy, V. Srinivasan, Magnesium and magnesium alloy hydrides, *International Journal of Hydrogen Energy*, 11, 169-192, 1986.

[20]   H. Chen, P. Liu, J. Li, Y. Wang, C. She, J. Liu, L. Zhang, Q. Yang, S. Zhou, X. Feng, MgH_2/Cu_xO Hydrogen storage composite with defect-rich surfaces for carbon dioxide hydrogenation, *ACS Applied Materials & Interfaces*, 11, 31009-31017, 2019.

[21]   N. Cheng, L. Zhang, K. Doyle-Davis, X. Sun, Single-atom catalysts: from design to application, *Electrochemical Energy Reviews*, 2, 539-573, 2019.

[22]   A.L. Maulana, R.I.D. Putra, A.G. Saputro, M.K. Agusta, Nugraha, H.K. Dipojono, DFT and microkinetic investigation of methanol synthesis via CO_2 hydrogenation on Ni(111)-based surfaces, *Physical Chemistry Chemical Physics*, 21, 20276-20286, 2019.

[23]   C.-M. Wang, Y.-D. Wang, J.-W. Ge, Z.-K. Xie, Reaction: industrial perspective on single-atom catalysis, *Chem*, 5, 2736-2737, 2019.

[24]   S. Okazaki, M. Kurimata, T. Iizuka, K. Tanabe, The effect of phosphoric acid treatment on the catalytic property of niobic acid, *Bulletin of the Chemical Society of Japan*, 60, 37-41, 1987.

[25]   J. William S. Wadsworth, Synthetic applications of phosphoryl-stabilized anions, *Organic Reactions*, 25, 77-145, 1977.

[26]   B. Delley, From molecules to solids with the DMol^3 approach, *The Journal of Chemical Physics*, 113, 7756-7764, 2000.

[27]   M. Huš, V.D.B.C Dasireddy, N. Strah Štefančič, B. Likozar, Mechanism, kinetics, and thermodynamics of carbon dioxide hydrogenation to methanol on $Cu/ZnAl_2O_4$ spinel-type heterogeneous catalysts, *Applied Catalysis B: Environmental*, 207, 267-278, 2017.

[28]   H. Chen, M. Yang, J. Liu, G. Lu, X. Feng, Insight into the effects of electronegativity on the H_2 catalytic activation for CO_2 hydrogenation: four transition metal cases from a DFT study, *Catalysis Science & Technology*, 10, 5641-5647, 2020.

[29]   B. Hammer, J.K. Nørskov, Theoretical surface science and catalysis—Calculations and concepts, *Advances in Catalysis*, 25, 71-129, 2000.

[30]   Z. Ou, J. Ran, J. Niu, C. Qin, W. He, L. Yang, A density functional theory study of CO_2 hydrogenation to methanol over Pd/TiO_2 catalyst: The role of interfacial site, *International Journal of Hydrogen Energy*, 45, 6328-6340, 2020.

[31]   L. Liu, F. Fan, M. Bai, F. Xue, X. Ma, Z. Jiang, T. Fang, Mechanistic study of methanol synthesis from CO_2 hydrogenation on Rh-doped Cu(111) surfaces, *Molecular Catalysis*, 466, 26-36, 2019.